Lijnen, H. R., van Hoef, B., & Collen, D. (1981) *Eur. J. Biochem. 120*, 149-154.
Longstaff, C., Campbell, A. F., & Fersht, A. R. (1990) *Biochemistry 29*, 7339-7347.
Moroi, M., & Aoki, N. (1976) *J. Biol. Chem. 251*, 5956-5965.
Morrison, J. F. (1982) *Trends Biochem. Sci. 7*, 102-105.
Morrison, J. F., & Walsh, C. T. (1988) *Adv. Enzymol. 61*, 201-301.
Mullertz, S., & Clemmensen, I. (1976) *Biochem. J. 159*, 545-553.
Nieuwenhuizen, W., & Traas, D. W. (1989) *Thromb. Haemostasis 61*, 208-210.
Ohlsson, K., & Laurell, C.-B. (1976) *Clin. Sci. Mol. Med. 51*, 87-92.
Potempa, J., Shieh, B.-H., & Travis, J. (1988) *Science 241*, 699-700.
Read, R. J., & James, M. N. G. (1986) in *Proteinase Inhibitors* (Barret, A. J., & Salvesen, G., Eds.) pp 301-336, Elsevier, Amsterdam.
Richarz, R., Tschesche, H., & Wurtrich, K. (1980) *Biochemistry 19*, 5711-5715.
Rühlhman, A., Kukla, D., Schwagen, P., Bartels, K., & Huber, R. (1973) *J. Mol. Biol. 77*, 417-436.
Schägger, H., & Von Jagow, G. (1987) *Anal. Biochem. 166*, 368-379.
Schechter, I., & Berger, A. (1967) *Biochem. Biophys. Res. Commun. 27*, 157-162.
Shapiro, R., & Riordan, J. F. (1984) *Biochemistry 23*, 5234-5240.
Shieh, B.-H., Potempa, J., & Travis, J. (1989) *J. Biol. Chem. 264*, 13420-13423.
Travis, J., & Salvesen, G. S. (1983) *Annu. Rev. Biochem. 52*, 655-709.
Tsou, C. L. (1988) *Adv. Enzymol. 61*, 381-436.
Wiman, B. (1981) *Methods Enzymol. 80*, 395-408.
Wiman, B., & Collen, D. (1978) *Eur. J. Biochem. 84*, 573-578.
Wiman, B., & Collen, D. (1979) *J. Biol. Chem. 254*, 9291-9297.
Wiman, B., Boman, L., & Collen, D. (1978) *Eur. J. Biochem. 87*, 143-146.

Analysis of ϕ and χ_1 Torsion Angles for Hen Lysozyme in Solution from ^{1}H NMR Spin-Spin Coupling Constants†

Lorna J. Smith, Michael J. Sutcliffe,‡ Christina Redfield, and Christopher M. Dobson*
Oxford Centre for Molecular Sciences and Inorganic Chemistry Laboratory, University of Oxford, South Parks Road, Oxford OX1 3QR, England

Received July 30, 1990; Revised Manuscript Received October 8, 1990

ABSTRACT: Three-bond $^3J_{HN\alpha}$ coupling constants have been determined for 106 residues and $^3J_{\alpha\beta}$ coupling constants have been measured for 57 residues of the 129-residue protein hen egg white lysozyme. These NMR data have been compared with torsion angles defined in the tetragonal and the triclinic crystal forms of the protein. For most residues the measured $^3J_{HN\alpha}$ values were consistent with the ϕ torsion angles found in both crystal forms; the RMS difference between the coupling constants calculated by using the tetragonal crystal structure ϕ angles and the experimental $^3J_{HN\alpha}$ values is 0.88 Hz. Thus there appears to be no significant averaging of the ϕ torsion angle either in the interior or at the surface of the protein. For 41 of the residues where $^3J_{\alpha\beta}$ coupling constants have been determined, the values are consistent with a single staggered conformation about the χ_1 torsion angle and there is complete agreement between the NMR data in solution and the torsion angles defined in the crystalline state. In contrast, for the other 16 residues where $^3J_{\alpha\beta}$ coupling constant values have been measured, the data indicate extensive motional averaging about the χ_1 torsion angle. These residues occur largely on the surface of the protein and examination of the crystal structures shows that many of these residues adopt a different conformation in the triclinic and tetragonal crystal forms and have high crystallographic temperature factors. It appears, however, that in solution conformational flexibility of the side chains of surface residues is significantly more pronounced than in individual crystal structures.

Developments in NMR[1] spectroscopy in recent years have made it possible to begin systematic comparisons between the structures and dynamic properties of proteins in solution and crystalline states (Clore & Gronenborn, 1987; Billeter et al., 1989). The study of the main-chain conformations of proteins is particularly favorable both by crystallographic techniques and by NMR spectroscopy. In the case of X-ray crystallography, the continuous density associated with the polypeptide chain enables it to be traced through the electron density map provided that the map is of sufficiently high resolution (Blundell & Johnson, 1976). From NMR spectroscopy, nu-

† This work was supported by the U.K. Science and Engineering Research Council.
* To whom correspondence should be addressed.
‡ Present address: Biological NMR Centre, Medical Sciences Building, Leicester University, University Road, Leicester LE1 9HN, U.K.

[1] Abbreviations: NMR, nuclear magnetic resonance; NOE, nuclear Overhauser enhancement; COSY, two-dimensional *J*-correlated spectroscopy; DQF COSY, two-dimensional double quantum filtered correlation spectroscopy; E. COSY, two-dimensional exclusive correlation spectroscopy; NOESY, two-dimensional nuclear Overhauser enhancement spectroscopy; RMS, root mean square.

0006-2960/91/0430-986$02.50/0

clear Overhauser effects are often very readily identified for main-chain C^α and amide protons, and their interpretation in terms of structural motifs is well understood (Wüthrich, 1986). In addition, dynamic properties of the main chain are also revealed particularly clearly from studies of amide proton exchange behavior (Wagner & Wüthrich, 1986) and from ^{13}C and ^{15}N relaxation measurements of main-chain C^α and amide nitrogen atoms (Kay et al., 1989).

By contrast, the characterization of side-chain conformations is significantly more difficult. Nevertheless it is an important objective since the side chains are clearly crucial for determining the structure of active sites, regions of surface contact, or interactions important for the folding of the protein. The functional significance of individual side chains in such cases may often be revealed by site-specific mutagenesis experiments, the interpretation of which must be related to the structural preference of the individual residues (Leatherbarrow & Fersht, 1986). In crystallographic studies, interpretation of electron density maps is often less straightforward for side chains, particularly when multiple conformations exist; such situations have been increasingly found as structures are refined to higher resolution (Smith et al., 1986). In the case of NMR studies, nuclear Overhauser effects are often harder to observe in crowded regions of 2D spectra where many side-chain proton resonances are found, and they are harder to interpret because of the larger number of conformational states potentially accessible for many side chains. Major difficulties in interpretation also result from the existence of multiple conformational states or dynamic averaging. The measurement of coupling constants is therefore of particular significance, especially in combination with nuclear Overhauser measurements or indeed crystallographic data, as it offers the opportunity, at least in principle, to examine populations about individual torsion angles (Nagayama & Wüthrich, 1981: Delepierre et al., 1982; Hoch et al., 1985; Hyberts et al., 1987).

Hen egg white lysozyme, an enzyme of 129 amino acids, has already been studied extensively by a wide variety of physical techniques. Of particular importance to this work are the detailed NMR spectroscopy studies, which have enabled ^{1}H NMR resonance assignments to be made for all the main-chain protons and for 70% of the side-chain protons of the protein (Redfield & Dobson, 1988; C. Redfield, unpublished results), and the high-resolution crystal structures, which have been determined by using X-ray and neutron diffraction techniques (Blake et al., 1967; Hodsdon et al., 1975; Mason et al., 1984; Handoll, 1985). In this paper we describe an analysis of NH–C^αH and C^αH–C^βH coupling constant data for many of the residues of hen lysozyme; these coupling constants are a function of the ϕ and χ_1 torsion angles, respectively. The data are compared with structural and dynamic information from high-resolution crystallographic studies of the protein in two distinct forms.

Materials and Methods

(*a*) *Acquiring the NMR Data.* Hen lysozyme was obtained from the Sigma Chemical Co. and samples were prepared by using the methods outlined by Redfield and Dobson (1988); all contained 7 mM protein at pH 3.8 and spectra were recorded at temperatures between 35 and 55 °C. Nonexchanged samples in 90% H_2O/10% D_2O were used in the COSY and E. COSY experiments for the determination of NH–C^αH coupling constants, while fully exchanged samples in D_2O were used in the E. COSY and DQF COSY experiments for the measurement of the C^αH–C^βH coupling constants. For the NOESY experiments used in the stereospecific assignment procedure, partly exchanged and reverse-exchanged samples were used to reduce the problems of measuring intensities when peaks overlap.

The NMR experiments were performed on the home-built 500-MHz spectrometer of the Oxford Centre for Molecular Sciences. The spectrometer is equipped with an Oxford Instruments Co. superconducting magnet, a GE/Nicolet 1280 computer and 293D pulse programmer, and a Bruker probe. Phase-sensitive *J*-correlated spectroscopy (COSY) (Aue et al., 1976; Bax & Freeman, 1981), double quantum filtered correlation spectroscopy (DQF COSY) (Rance et al., 1983), exclusive correlation spectroscopy (E. COSY) (Griesinger et al., 1987), and nuclear Overhauser enhancement spectroscopy (NOESY) (Jeener et al., 1979; Anil Kumar et al., 1980) experiments were performed according to the method of States et al. (1982) with standard phase cycling schemes. For the COSY experiments 512 t_1 increments of 4K complex data points were collected with a sweep width of 5618 Hz. Data sets consisting of 512 t_1 increments of 2K complex data points were collected for the DQF COSY and E. COSY experiments, using a sweep width of 5405.4 Hz in both cases. For the NOESY experiments, 256 t_1 increments of 1K complex data points were collected with a sweep width of 7042 Hz in both dimensions. A mixing time of 50 ms, randomly varied by 10% (Macura et al., 1981), was employed for the NOESY experiment. All spectra were resolution enhanced in t_2 by trapezoidal and double-exponential multiplication and in t_1 by trapezoidal multiplication. All data sets were zero-filled once in t_2 and twice in t_1. After zero filling, the digital resolution of the E. COSY and DQF COSY spectra in F_2 was 1.32 Hz/point and the digital resolution of the COSY experiment was 0.69 Hz/point.

(*b*) *Techniques for Coupling Constant Determination.* For a protein the size of lysozyme the line widths of ^{1}H NMR resonances are largely in excess of 5 Hz and frequently comparable to the value of the three-bond spin–spin coupling constants. This means that accurate values for coupling constants cannot be obtained directly from the splitting in conventional 2D COSY spectra, as the observed splittings between antiphase components becomes increasingly different from the true splittings with increasing line widths (Neuhaus et al., 1985). Two methods, the use of spectral simulations and the measurement of coupling constants from cross peaks in E. COSY spectra, were used to overcome this problem.

For the NH–C^αH coupling constants of all non-glycine residues the antiphase splittings in COSY cross sections parallel to F_2 were measured and the distortions arising from the finite line widths were corrected for by using spectral simulations. Cross sections simulated by applying appropriate resolution enhancement functions to antiphase Lorentzian doublets were fitted to experimental cross sections parallel to F_2 through the NH–C^αH cross peaks (Redfield & Dobson, 1990).

Test calculations on simulated data with varying signal-to-noise levels show that the fitting procedure works well for cross sections that have a signal-to-noise ratio (for resolution enhanced spectra) of 4:1 or better. At worse signal-to-noise levels the fitting procedure is less satisfactory and an alternative procedure was adopted. The observed splitting between the positive and negative components of an antiphase doublet can arise from various combinations of coupling constant and line width. Spectra were simulated for several pairs of coupling constant and line width values that give the experimentally observed splitting (the line width was varied in 1-Hz increments). Then these simulated spectra were compared with the pair of experimental cross sections, and the combination

Table I: Observed NH–C$^{\alpha}$H Antiphase Splittings, Corrected NH–C$^{\alpha}$H Coupling Constants, and NH Line Widths for Several Residues of Hen Egg White Lysozyme at Three Temperatures[a]

	35 °C			45 °C			55 °C		
residue	J_{obs}	J_{corr}	LW	J_{obs}	J_{corr}	LW	J_{obs}	J_{corr}	LW
Met 12	6.5	4.5	11.0	5.8	4.8	8.6	5.6	4.5	8.1
Ser 91	6.7	5.5	9.6	6.1	5.5	8.0	5.9	5.5	7.0
Ala 107	5.6	4.4	9.2	5.2	4.2	7.4	4.8	4.2	6.6
Thr 43	9.5	9.3	9.6	9.2	9.3	7.6	9.2	9.3	7.0
Arg 68	9.8	9.6	9.1	9.7	9.7	7.3	9.7	9.7	6.2
Leu 129	9.0	9.0	6.9	9.0	9.0	5.8	9.0	9.1	4.5

[a] J_{obs} is the observed NH–C$^{\alpha}$H antiphase splitting. J_{corr} and LW are the corrected NH–C$^{\alpha}$H coupling constant and the line width of the NH resonance obtained from computer fits as described under Materials and Methods. All values are in hertz with an accuracy ±0.5 Hz. A range of NH line widths has been observed but the majority lie in the range 9.0 ± 1.0 Hz at 35 °C.

of coupling constant and line width that gave the best agreement with the experimental data was selected. For cross sections with good signal-to-noise levels this method and the fitting procedure gave comparable results. Similar methods were used to extract the true C$^{\alpha}$H–C$^{\beta}$H coupling constant values for Thr, Val, and Ile residues from the observed antiphase splittings in C$^{\alpha}$H–C$^{\beta}$H cross peaks in the DQF COSY spectrum.

For the NH–C$^{\alpha}$H coupling constants of glycine residues and the C$^{\alpha}$H–C$^{\beta}$H coupling constants of all residues with two protons bonded to the β carbon, the values were determined as passive coupling constants, where possible, from the relative displacement of the cross-peak components in E. COSY NH–C$^{\alpha}$H, C$^{\alpha}$H–C$^{\beta}$H, or C$^{\beta}$H–C$^{\beta}$H cross peaks (Griesinger et al., 1987). This relative displacement is independent of the line width and so can be used to give the coupling constant values directly. In some cases where only one of the C$^{\alpha}$H–C$^{\beta}$H cross peaks could be observed (the other C$^{\alpha}$H–C$^{\beta}$H cross peak overlapping with other peaks or being too close to the diagonal to be studied) one of the coupling constants could only be measured as an active coupling constant. In these cases, the true coupling constant value was then determined from the observed splitting by using spectral simulations.

(*c*) *Use of Crystal Structures.* Coordinates for hen lysozyme were taken from the 2.0-Å resolution tetragonal type 2 crystal structure obtained by X-ray diffraction (Handoll, 1985) and the 1.4-Å resolution triclinic crystal structure obtained by neutron diffraction and provided by Dr. Sax Mason (Grenoble). (The *R* factors for these structures are 0.22 and 0.18, respectively.) The predicted coupling constant values were calculated from the crystal structures by using (Karplus, 1959)

$$^3J = A\cos^2\theta + B\cos\theta + C$$

where $\theta = \phi - 60°$ for $^3J_{HN\alpha}$, $\theta = \chi_1 - 120°$ for Hβ_2, and $\theta = \chi_1$ for Hβ_3 [Hβ_2 and Hβ_3 are defined according to the IUPAC-IUB conventions (1970)]. Values for *A*, *B*, and *C* of 6.4, −1.4, and 1.9 for $^3J_{HN\alpha}$ (Pardi et al., 1984) and 9.5, −1.6, and 1.8 for $^3J_{\alpha\beta}$ (de Marco et al., 1978) were used. For Ser and Thr the effects of the high electronegativity of oxygen were corrected for by dividing the calculated $^3J_{\alpha\beta}$ values by 1.08 (Kopple et al., 1973).

Results

(*a*) *Coupling Constant Determination.* NH–C$^{\alpha}$H coupling constants were measured for lysozyme at three temperatures, 35, 45, and 55 °C. The antiphase splittings measured from the COSY spectra and the coupling constants and line widths determined by the splitting program are summarized in Table I for several residues of lysozyme, and in Figure 1 the experimental cross sections are compared with the best-fit simulations for two representative residues, Thr 43 and Ala 107. The measured splittings at the three temperatures are quite different for residues such as Met 12, Ser 91, and Ala 107. All these residues have measured splittings that decrease significantly as the temperature is increased from 35 to 55 °C. The coupling constants obtained for these residues from the fitting procedure are all smaller than the values measured directly from the spectra; the values obtained for the three temperatures are, however, very similar. As expected the line widths obtained from the simulations decrease as the temperature is increased. These residues all have relatively small $^3J_{HN\alpha}$ values characteristic of α-helical secondary structure. It is clear that for residues with these small coupling constants the correction for distortion due to resonance line width is necessary before the true coupling constant can be obtained. In contrast, the measured splittings for residues such as Thr 43, Arg 68, and Leu 129 do not vary significantly with tem-

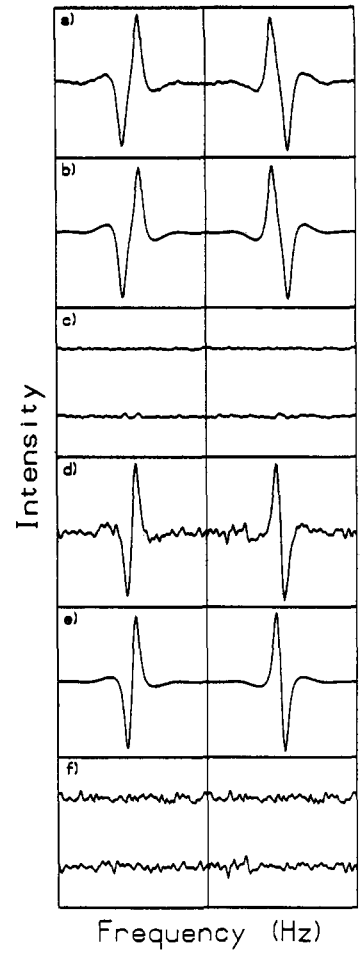

FIGURE 1: Examples of the computer fitting procedure for Thr 43 and Ala 107 at 55 °C. (a) The pair of experimental COSY cross sections parallel to F_2 through the NH–C$^{\alpha}$H peak of Thr 43. The observed antiphase splitting is 9.2 Hz. (b) Best computer fitted simulation for Thr 43 obtained with J = 9.3 Hz and LW = 7.0 Hz. (c) The lower traces show the difference between the experimental cross section of Thr 43 (a) and the best-fit simulation (b). The upper traces show the noise level of the experimental data. (d) The pair of experimental COSY cross sections parallel to F_2 through the NH–C$^{\alpha}$H peak of Ala 107. The observed antiphase splitting is 4.8 Hz. (e) Best computer fitted simulation for Ala 107 obtained with J = 4.2 Hz and LW = 6.6 Hz. (f) The lower traces show the difference between the experimental cross section of Ala 107 (d) and the best-fit simulation (e). The upper traces show the noise level of the experimental data. The difference in signal-to-noise between (a) and (d) is a result of the difference in NH–C$^{\alpha}$H coupling constants for Thr 43 and Ala 107. The total frequency range in each cross section is 88 Hz.

Table II: NH–C$^\alpha$H Coupling Constants for Hen Egg White Lysozyme, ϕ Torsion Angles from the Tetragonal Type 2 and Triclinic Crystal Structures, and Minimum Calculated ϕ Differences between Experimental and Crystal Data[a]

residue	coupling const	tetragonal ϕ	triclinic ϕ	$\phi_{expt} - \phi_{tetr}$	$\phi_{expt} - \phi_{tric}$	residue	coupling const	tetragonal ϕ	triclinic ϕ	$\phi_{expt} - \phi_{tetr}$	$\phi_{expt} - \phi_{tric}$
Val 2	10.0	−102.7	105.2	−17.3	−14.8	Cys 64	8.8	−151.8	−129.8	11.0	−11.0
Phe 3	7.4	−76.4	−79.3	−9.1	−6.2	Asn 65	9.4	−103.0	−98.3	−5.1	−9.8
Gly 4	6.1, 8.0	−93.7	−77.3			Asp 66	10.0	−116.9	−109.2	−3.1	−10.8
Cys 6	5.8	−66.4	−74.1	−6.4	1.3	Gly 67	5.5, 6.2	65.4	85.2		
Glu 7	4.5	−59.6	−58.3	−2.9	−4.2	Arg 68	9.7	−139.5	−115.4	19.5	−4.6
Leu 8	5.5	−67.6	−71.3	−2.9	0.8	Thr 69	9.3	−120.3	−98.2	−13.7	−8.0
Ala 9	3.7	−55.7	−50.5	0.0	−5.1	Gly 71	5.7, 5.9	54.1	73.7		
Ala 10	3.9	−65.8	−69.4	8.4	12.0	Cys 76	8.8	−88.6	−86.7	−10.6	−12.5
Ala 11	4.8	−70.6	−67.8	5.6	2.9	Asn 77	7.4	52.9	60.4	7.1	−0.4
Met 12	4.6	−67.2	−64.8	3.9	1.5	Ile 78	8.0	−152.9	−145.4	3.7	−3.8
Lys 13	4.2	−58.4	−69.0	−1.6	9.0	Cys 80	3.6	−53.0	−59.4	−1.6	4.8
Arg 14	4.4	−61.5	−69.7	−0.2	8.0	Ser 81	3.6	−60.6	−68.6	6.0	13.9
His 15	9.2	−88.7	−87.2	−16.0	−17.5	Ala 82	5.4	−63.4	−63.8	−6.2	−5.9
Gly 16	6.1, 6.2	81.1	72.9			Leu 83	7.2	−84.6	−86.4	0.8	2.6
Leu 17	7.6	−82.0	−84.9	−5.2	−2.3	Leu 84	9.2	−104.4	−107.4	−0.2	2.7
Asp 18	5.7	−64.7	−65.3	−7.3	−6.7	Ser 85	5.8	−72.4	−72.2	−0.4	−0.5
Asn 19	7.0	69.4	70.3	−9.4	−10.3	Ser 86	5.8	−64.5	−72.0	−8.3	−0.7
Tyr 20	5.5	−61.8	−70.0	−8.6	−0.4	Asp 87	8.9	−84.6	−82.3	−15.8	−18.1
Arg 21	6.8	60.4	51.3	7.2	1.1	Ile 88	6.5	−76.0	−86.9	−2.2	8.7
Gly 22	6.0, 6.8	85.4	79.8			Ala 90	4.2	−60.7	−62.7	0.7	2.7
Tyr 23	8.6	−99.0	−109.8	2.2	12.9	Ser 91	5.5	−62.7	−68.6	−7.7	−1.9
Gly 26	3.3, 6.2	−58.2	−57.9			Val 92	5.6	−60.9	−67.9	−10.3	−3.4
Asn 27	5.4	−65.7	−58.9	−3.9	−10.8	Asn 93	4.4	−59.8	−57.4	−1.8	−4.3
Trp 28	6.0	−61.0	−67.3	−13.3	−7.0	Cys 94	6.3	−74.1	−71.1	−2.5	−5.5
Val 29	5.9	−68.1	−67.9	−5.4	−5.6	Lys 96	4.4	−56.7	−64.2	−5.0	2.5
Cys 30	3.8	−62.1	−61.4	5.5	4.9	Lys 97	6.5	−67.6	−65.8	−10.6	−12.4
Ala 31	3.8	−60.6	−63.6	4.1	7.1	Val 99	5.2	−60.7	−72.4	−7.4	4.3
Ala 32	4.8	−62.4	−63.4	−2.5	−1.6	Asp 101	7.0	−65.4	−94.7	−16.8	12.5
Lys 33	3.6	−54.3	−60.1	−0.4	5.4	Gly 102	6.2, 6.4	161.5	67.0		
Phe 34	7.6	−78.3	−89.3	−8.9	2.1	Asn 103	8.2	−113.1	−107.7	20.4	14.9
Glu 35	7.2	−80.1	−79.9	−3.7	−3.9	Gly 104	3.9, 6.4	57.5	−83.6		
Ser 36	9.6	−135.5	−134.7	8.7	7.9	Met 105	7.4	−70.5	−77.2	−15.0	−8.3
Phe 38	6.3	69.4	68.7	9.6	10.3	Ala 107	4.2	−60.7	−55.7	0.7	−4.3
Asn 39	8.8	−100.4	−93.0	1.2	−6.1	Trp 108	9.6	−108.0	−93.9	−5.2	−19.3
Thr 40	5.4	−66.8	−67.3	−2.9	−2.4	Val 109	4.0	−48.3	−61.1	−10.0	2.8
Gln 41	9.2	−88.6	−96.9	−16.1	−7.7	Trp 111	7.1	−69.3	−61.0	−13.7	−22.0
Ala 42	4.5	−62.5	−62.9	0.0	0.4	Arg 112	4.5	−58.9	−62.9	−3.6	0.4
Thr 43	9.3	−139.1	−129.5	5.4	−4.2	Asn 113	5.8	−83.0	−89.9	10.3	17.2
Asn 44	9.4	−154.0	−126.2	22.1	−5.7	Arg 114	9.6	−121.8	−127.8	−5.0	1.0
Arg 45	7.7	−93.6	−91.1	5.5	3.0	Cys 115	9.8	−119.0	−118.8	−1.0	−1.2
Asn 46	8.8	−105.7	−92.2	6.5	−7.0	Gly 117	6.2, 6.5	73.2	84.7		
Thr 47	4.4	−62.9	−80.7	1.2	19.0	Thr 118	9.8	−107.6	−90.8	−12.4	−29.2
Asp 48	7.7	−74.8	−87.8	−13.3	−0.3	Asp 119	6.7	−85.7	−79.4	5.9	−0.4
Gly 49	5.3, 8.0	91.3	91.3			Val 120	4.6	−60.0	−58.4	−3.3	−4.9
Ser 50	7.8	−82.9	−97.2	−6.1	8.2	Gln 121	5.0	−59.1	−53.9	−7.4'	−12.6
Thr 51	9.8	−139.6	−131.3	19.6	11.3	Ala 122	3.7	−60.7	−53.9	5.1	−1.7
Asp 52	9.6	−100.8	−98.6	−12.4	−14.6	Trp 123	5.4	−65.9	−70.1	−3.7	0.4
Tyr 53	9.6	−126.6	−117.1	−0.2	3.9	Ile 124	10.6	−114.6	−113.0	−5.4	−7.0
Leu 56	9.7	−111.1	−113.5	−8.9	−6.5	Arg 125	4.4	−62.7	−68.1	1.0	6.5
Gln 57	6.3	45.2	54.5	−4.2	−13.5	Gly 126	5.6, 6.8	81.5	81.4		
Ile 58	8.0	−78.2	−84.9	−12.6	−5.9	Cys 127	7.7	−85.0	−101.0	−3.1	12.9
Ser 60	5.1	−74.5	−83.1	7.2	15.8	Arg 128	8.0	−95.1	−71.8	4.3	−19.0
Arg 61	6.2	−69.5	−75.9	−6.4	0.0	Leu 129	9.0	−124.0	−165.5	−14.3	27.2

[a] The coupling constants given in this table are the average of the 45 and 55 °C corrected coupling constants; the 35 °C value was used only if no other measurement was possible. Corrected coupling constants were obtained from computer fits as described under Materials and Methods; values are in hertz. Stereospecific assignments for glycine C$^\alpha$H have not been made. The ϕ torsion angles and the difference in ϕ are given in degrees.

perature. The coupling constants obtained for these residues from the fitting procedure are almost the same as the measured splittings. All these residues have relatively large coupling constants characteristic of extended structure. As was found for the residues with small $^3J_{HN\alpha}$ values, the line widths for these resonances decrease as the temperature is increased. Average coupling constant values for 106 of the 129 residues of lysozyme are listed in Table II and full details of the coupling constant measurements at each of the three temperature are listed as supplementary material.

For the measurement of C$^\alpha$H–C$^\beta$H coupling constants, for residues with an AMX-type spin system (residues where the two protons attached to the β carbon are not spin–spin coupled to any protons in the γ group, e.g., Asn, Ser, and Tyr) and certain residues (e.g., Arg and Lys) with more complex spin systems the problems of finite line widths were overcome by using the E. COSY experiment. For hen lysozyme, pairs of $^3J_{\alpha\beta}$ values were measured for these residues in all cases where the relevant cross peaks could be resolved. A total of 35 pairs of values have been determined for residues with an AMX-type spin system and eight pairs for residues with more complex spin systems. Details are given in Table III and examples of the experimental cross sections indicating how the measurements were made are shown in Figure 2. For 29 residues, 67% of those studied, the values for the pairs of C$^\alpha$H–C$^\beta$H coupling constants were found either to be both less than 5 Hz or to differ from each other by more than 5 Hz. From the Karplus equation, the predicted $^3J_{\alpha\beta}$ values for a staggered

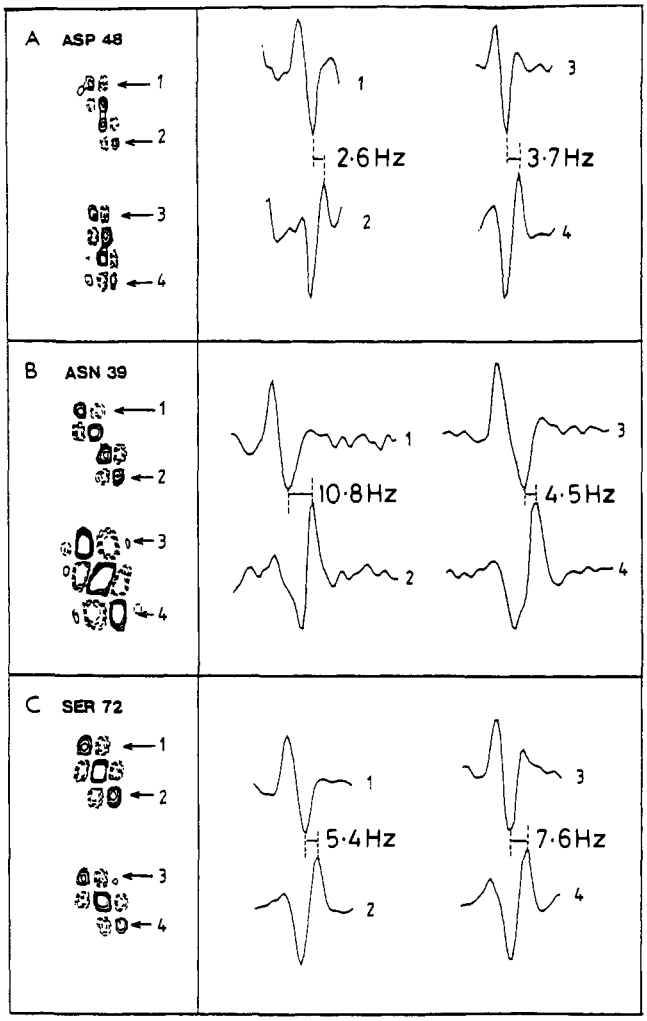

FIGURE 2: $C^{\alpha}H$–$C^{\beta}H$ cross peaks from the 500-MHz E. COSY spectrum of fully exchanged hen lysozyme with cross sections through the cross peaks showing how the $^3J_{\alpha\beta}$ values were measured for cases with (A) two small $^3J_{\alpha\beta}$ values, (B) one large and one small $^3J_{\alpha\beta}$ value, and (C) $^3J_{\alpha\beta}$ values averaged by large-scale motions. 1 and 2 show the cross sections through the cross peak for the C^{β} proton with the lower chemical shift, and 3 and 4 show the cross sections through the cross peak for the C^{β} proton with the higher chemical shift.

conformation about the $\alpha\beta$ bond are either both 3.4 Hz (for $\chi_1 = 60°$) or 12.9 and 3.4 Hz (for $\chi_1 = 180°, -60°$). Given the accuracy of the experimental measurements (of the order of 1 Hz), the assumptions made in the calculation of the J values, and the fact that even slight fluctuations around the average χ_1 value will reduce the observed value for large coupling constants and increase the observed value for small coupling constants (Hoch et al., 1985), we have assumed here that for these 29 residues the experimental results are consistent with a single staggered conformation.

The method outlined by Wagner et al. (1987) and Arseniev et al. (1988) was used to make stereospecific assignments for the residues placed in a single staggered conformation. The $C^{\alpha}H$–$C^{\beta}H$ spin–spin coupling constants and the relative intensities of the intraresidue NOESY cross peaks between the amide and C^{β} protons and between the C^{α} and C^{β} protons were compared with the patterns of these parameters that are expected for the three staggered rotamer positions [Figure 4 in Wagner et al. (1987)]. For the 23 residues where the experimental results were consistent with one of the predicted sets of values, the stereospecific assignments were made and the χ_1 dihedral angle was identified; full details are given in Table IV. In the other six cases either the NOESY cross-peak

Table III: $C^{\alpha}H$–$C^{\beta}H$ Coupling Constants for Hen Egg White Lysozyme and χ_1 Torsion Angles from the Tetragonal Type 2 and the Triclinic Crystal Structures[a]

residue	coupling const $\alpha\beta_A$[b]	coupling const $\alpha\beta_B$	method of measurement[c]	tetragonal χ_1	triclinic χ_1
Val 2	10.8		C	178.5	179.6
Phe 3	3.0[d]	10.0[d]	B	-84.9	-82.8
Cys 6	3.5	11.5	B	-68.2	-67.5
Glu 7[e]	6.7	6.4	A	-177.6	-65.7
Lys 13[e]	9.2	5.1	A	-157.8	-173.4
His 15	2.6	11.2	A	-84.0	-72.0
Asp 18	11.0	4.2	A	-166.2	-170.5
Asn 19[e]	6.4	7.3	A	-79.5	-161.1
Tyr 20	2.3	11.7	B	-172.8	179.7
Tyr 23	10.9	2.7	B	-70.6	-66.4
Asn 27	10.3	2.4	A	-78.9	-75.9
Trp 28	10.7	4.1	A	-64.5	-60.9
Val 29	11.1		C	175.0	178.6
Cys 30	10.8	5.3	B	-177.4	-173.5
Phe 34	5.0	10.7	B	-58.0	-67.1
Asn 37[e]	8.1	4.2	A	-161.4	-152.0
Asn 39	10.8	4.5	A	-172.3	-172.5
Thr 40	4.5		C	67.3	59.4
Thr 43	3.7		C	62.7	60.5
Arg 45[e]	6.9	6.7	A	-175.1	-66.4
Asn 46	4.7	11.2	A	-49.8	-60.9
Thr 47	2.6		C	52.4	61.5
Asp 48	2.6	3.7	A	70.0	70.3
Thr 51	9.3		C	-55.8	-62.1
Asp 52	11.6	3.6	A	-61.4	-55.5
Tyr 53	10.4	3.0	B	-63.6	-69.8
Asn 59	5.4	11.3	A	-168.8	-179.1
Arg 61	10.8	5.7	B	-175.5	-168.3
Cys 64	2.7	4.6	A	63.6	67.3
Asn 65	11.4	4.5	A	177.5	-170.7
Asp 66	5.1	4.5	A	65.5	64.2
Arg 68[e]	4.8	6.5	A	68.1	-66.0
Thr 69	9.3		C	-43.7	-57.8
Ser 72[e]	5.4	7.6	A	-152.0	-165.0
Asn 74	10.5	3.9	A	-154.9	-168.6
Leu 75	12.4	2.1	A	-87.5	-63.3
Asn 77[e]	8.3	5.9	A	-168.2	-162.2
Ser 85[e]	5.7	7.4	A	131.4	-166.8
Ser 86[e]	6.4	4.1	A	-69.5	-54.6
Asp 87	11.5	5.1	B	-177.6	150.4
Ile 88	4.5		C	74.9	66.0
Thr 89	9.5		C	-54.6	-63.5
Val 92	10.1		C	162.3	167.1
Asn 93	10.8	3.5	A	-74.3	-67.4
Cys 94	4.0	12.2	A	-173.6	-174.5
Val 99[e]	6.3		C	80.3	171.1
Ser 100[e]	7.7	4.0	A	-52.4	-47.3
Asp 101[e]	6.6	5.6	A	-151.4	-97.9
Asn 106	10.5	3.6	A	-68.7	-70.4
Val 109[e]	8.0		C	67.5	38.2
Thr 118	4.2		C	69.8	70.9
Asp 119	11.7	4.9	A	173.5	-175.6
Trp 123	2.9	10.6	A	-69.0	-68.9
Ile 124	4.6		C	57.2	64.3
Arg 125[e]	7.9	6.1	A	-52.0	166.4
Cys 127	4.8	11.6	B	-53.5	-58.2
Arg 128[e]	7.2	7.9	A	170.9	-86.3

[a] Coupling constant values are in hertz (error approximately ±1 Hz) and the χ_1 angles are given in degrees. For Val, Thr, and Ile the $^3J_{\alpha\beta}$ values were determined from spectra run at 55 °C. For all other residues the values were determined from spectra run at 35 °C. [b] In this work β_A and β_B are defined as the proton attached to the β carbon whose resonance has the higher and lower chemical shift, respectively. For residues with only one β proton the values are listed under β_A. [c] Method of coupling constant measurement: (A) Values measured as passive coupling constants from the E. COSY spectrum. (B) One or both values determined by simulations using active coupling constant values from the E. COSY spectrum. (C) Value measured from splitting in DQF COSY cross peaks and corrected for line width effects by using simulations. [d] Values are only approximate. [e] Residues identified as not occupying a single staggered conformation about χ_1 by using the criteria listed in the text.

Table IV: Details of the Experimentally Determined $C^\alpha H-C^\beta H$ Coupling Constants, the Relative NOESY Cross-Peak Intensities for the Intraresidue $NH-C^\beta H$ and $C^\alpha H-C^\beta H$ Cross Peaks, and the Resulting Stereospecific Assignments

	coupling const (Hz)		rel NOE intensities[b]					stereospecific assignment	
residue	$\alpha\beta_A$[a]	$\alpha\beta_B$	NH-Hβ_A	NH-Hβ_B	Hα-Hβ_A	Hα-Hβ_B	approx χ' values	β_2	β_3
Phe 3	~3	~10	5	16	12	2	−60°	β_B	β_A
Cys 6	3.5	11.5	8	16	5	4	−60°	β_B	β_A
His 15	2.6	11.2	8	16		8	−60°	β_B	β_A
Asp 18	11.0	4.2	16	11	4	11	180°	β_B	β_A
Tyr 20	2.3	11.7	11	11	16	4	180°	β_A	β_B
Tyr 23	10.9	2.7	8	4		5	−60°	β_A	β_B
Asn 27	10.3	2.4	16	5			−60°	β_A	β_B
Cys 30	10.8	5.3	16	16			180°	β_B	β_A
Phe 34	5.0	10.7	1	11	16	8	−60°	β_B	β_A
Asn 39	10.8	4.5	11	11	4	5	180°	β_B	β_A
Asn 46	4.7	11.2	4	8			−60°	β_B	β_A
Asp 48	2.6	3.7	2	8			60°	β_A	β_B
Asp 52	11.6	3.6	11	1	2		−60°	β_A	β_B
Tyr 53	10.4	3.0	8	4	2	5	−60°	β_A	β_B
Asn 59	5.4	11.3	8	8	8	2	180°	β_A	β_B
Arg 61	10.8	5.7	11	11			180°	β_B	β_A
Asp 66	5.1	4.5	1	2	16	16	60°	β_A	β_B
Leu 75	12.4	2.1	16	2	4	8	−60°	β_A	β_B
Asp 87	11.5	5.1	11	11	5		180°	β_B	β_A
Cys 94	4.0	12.2	11	11	11		180°	β_A	β_B
Asp 119	11.7	4.9	11	11	24	34	180°	β_B	β_A
Trp 123	2.9	10.6	4	8	11	4	−60°	β_B	β_A
Cys 127	4.8	11.6	1	4	16	11	−60°	β_B	β_A

[a] β_A and β_B are defined as the C^β proton whose resonance has the higher and lower chemical shift, respectively. [b] The relative NOESY cross-peak intensities are given in terms of relative peak heights determined by counting the number of contour levels. Direct comparisons between the NH-$C^\alpha H$ and the $C^\alpha H-C^\beta H$ NOE intensities are not possible as the measurements were made from different spectra.

intensities could not be measured due to peak overlap or their relative intensities were ambiguous.

The values of the measured $C^\alpha H-C^\beta H$ coupling constants for the remaining 14 residues studied here are not consistent with the side chains of these residues being present in a single staggered conformation in solution. For the majority of these cases both the measured coupling constants are in the range 5–8 Hz. For residues with two C^β protons this requires that the coupling constants are averaged due to motion between two or more conformations populated by the side chain in solution (Nagayama & Wüthrich, 1981; Hoch et al., 1985). For completely free rotation about the $\alpha\beta$ bond both coupling constant values are predicted (from the Karplus equation) to be ~6.6 Hz.

For Val, Thr, and Ile residues, where only one proton is attached to the β carbon, the side chain is assumed to adopt a single staggered conformation when the measured coupling constant is greater than 10 Hz (greater than 9 Hz for Thr because of the effects of the high electronegativity of the oxygen substituent) or less than 5 Hz. Twelve out of the 14 residues studied fit into this category. For cases where the measured coupling constant does not fulfill this requirement (two residues here, Val 99 and Val 109), the results could either represent occupation of a nonstaggered conformation or population of multiple conformations. For Val 109, evidence for the rotational mobility of the side chain has been obtained previously from the broadening of resonances on the binding of Gd(III) to the protein (Campbell et al., 1975). Val 99 is discussed further later in this paper.

(b) Comparisons between the Solution and Crystallographic Structures. $^3J_{HN\alpha}$ values calculated for lysozyme, using the ϕ angles from the 2.0-Å resolution tetragonal type 2 crystal structure and the 1.4-Å resolution triclinic crystal structure, are summarized in Figure 3, which shows plots of the coupling constants calculated from these two crystal structure versus the experimental $^3J_{HN\alpha}$ values. The agreement between the experimental and calculated data is excellent; an RMS difference of 0.88 Hz and a correlation coefficient of 0.97 is obtained for the tetragonal structure and an RMS difference of 0.93 and a correlation coefficient of 0.96 for the triclinic structure. The slope of the least-squares line fitted to the data is 0.99 for tetragonal and 0.98 for triclinic lysozyme. For 82 residues in the tetragonal structure and 78 in the triclinic structure the agreement between the experimental and calculated coupling constants is better than 1 Hz. The residues for which worse agreement is obtained are scattered throughout the sequence and vary to some extent between the two crystal structures. For 24 residues in the tetragonal structure and 28 in the triclinic structure the difference between the experimental and calculated coupling constants is greater than 1 Hz. For only 11 of these residues (~40%) are differences of greater than 1 Hz found for both the tetragonal and triclinic structures. In many cases good agreement is found between the experimental and calculated coupling constant for a particular residue in one structure and poor agreement for that residue in the other structure. For example, a difference of −1.9 Hz between the calculated and experimental coupling constants of Asn 44 is found when the tetragonal structure is used, whereas a difference of only 0.2 Hz is found when the triclinic structure is used. For Arg 128 a difference of −2.3 Hz is found for the triclinic structure, while a difference of only 0.4 Hz is found for the tetragonal structure. Such examples may indicate that the average structure of lysozyme in solution resembles more closely that of the tetragonal crystal structure in some regions of the protein and that of the triclinic crystal structure in other regions. For Asp 101 a difference of −2.1 Hz between experimental and calculated coupling constants is found for the tetragonal structure and a difference of 1.4 Hz is found for the triclinic crystal structure; the experimental coupling constant of 7.0 Hz is closer to the average calculated coupling constant of 6.6 Hz than it is to the values obtained from either the tetragonal (4.9 Hz) or the triclinic (8.4 Hz) structures. Residues 100–102 in tetragonal lysozyme are characterized by high temperature factors for backbone atoms. If the coupling constants calculated from the tetragonal and the triclinic crystal structures

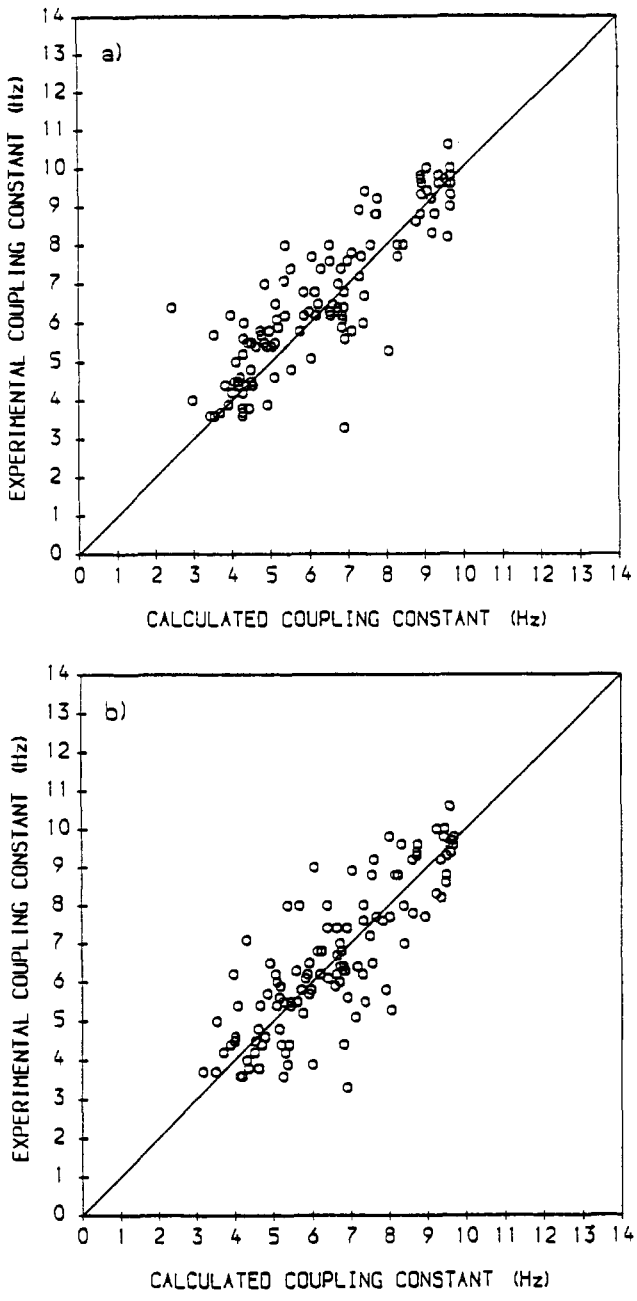

FIGURE 3: Plots of the experimental NH–C$^{\alpha}$H coupling constants versus the calculated coupling constants for $^{3}J_{HN\alpha}$ values calculated by using (a) ϕ torsion angles from the tetragonal type 2 crystal structure and (b) ϕ torsion angles from the triclinic crystal structure of hen lysozyme. Stereospecific assignments for glycine C$^{\alpha}$H have not been made. The calculated glycine coupling constants are plotted against the experimental coupling constants so as to give the the best agreement.

are averaged and compared with the experimental values, an RMS difference of 0.73 Hz is obtained. It is interesting to note that this RMS value is smaller than either of the values obtained from the tetragonal (0.88 Hz) or the triclinic (0.93 Hz) crystal structures alone. Although this may indicate the limitations of the present resolution of crystal structures, it is possible that for some residues the differences between the experimental and calculated coupling constants may result from some averaging of the ϕ torsion angle in solution.

The differences between the experimental and calculated coupling constants could in general arise from errors in the measurement of the coupling constants, from errors in the X-ray structures, or from real differences between the solution and X-ray structures. In order to explore the latter, the minimum differences in torsion angles needed to bring the experimental and calculated coupling constants into exact agreement have been determined; these are also listed in Table II for both the tetragonal and the triclinic structures. For 70 of the non-glycine residues in tetragonal lysozyme (66 in triclinic) the required difference in torsion angle is less than 10° and for only two residues (three in triclinic) is the difference more than 20° (10 residues >15° in the tetragonal and 13 residues >15° in the triclinic). Thus even without consideration of experimental errors only very small differences need to exist between the average backbone structure of hen lysozyme in the solution and crystalline states to explain the deviations from a perfect correlation in Figure 3.

In a similar way $^{3}J_{\alpha\beta}$ values were calculated, using the Karplus relationship, from the χ_1 torsion angles in the tetragonal type 2 and the triclinic crystal structures. Figure 4 shows plots of calculated versus experimental $^{3}J_{\alpha\beta}$ values from the tetragonal and triclinic crystal structure χ_1 data. For those cases where the experimental data are indicative of a single staggered conformation, the agreement between the experimental and calculated values is good for both structures. In addition, in every case where stereospecific assignments have been made, the same staggered rotamer is found to be adopted in solution and in both the crystal structures. If we consider just the data for these residues and compare the experimental and calculated $^{3}J_{\alpha\beta}$ values, the RMS difference is 1.48 with a correlation coefficient of 0.97 for the tetragonal data and 1.59 with a correlation coefficient of 0.97 for the triclinic data. The slope of the least-squares line fitted to the data is, however, only 0.74 for the tetragonal structure (0.73 for the triclinic) compared with a value of 0.99 for the $^{3}J_{HN\alpha}$ data. We return to discuss this point later.

For the residues with significantly averaged coupling constants the crystal structure χ_1 values are generally close to the values for staggered rotamers (χ_1 = 60°, −60°, 180°) (see Table III); in all but two cases, Ser 85 in the tetragonal and Asp 101 in the triclinic, the χ_1 values are within ±30° of a staggered value. As the experimental coupling constant values are averaged as a consequence of the population of multiple conformations, the agreement between the experimental and predicted set of $^{3}J_{\alpha\beta}$ values is poor. It is important to note here that the observation of a single resonance and C$^{\alpha}$H–C$^{\beta}$H coupling constant for each C$^{\beta}$ proton shows that fast exchange conditions are satisfied on the NMR time scale, indicating that the interconversion between the different conformations adopted by the side chain must occur at a rate of at least 20 Hz.

It is interesting to compare the χ_1 values found in the tetragonal type 2 and the triclinic crystal structures. For the residues that have been identified as having a well-defined χ_1 angle in solution the χ_1 values are closely similar, for 95% of the residues the difference being less than 15°. By contrast, for 8 of the 16 residues with averaged coupling constants there are major differences, the side chain adopting different rotameric forms in the two structures. For Glu 7, for example, χ_1 = −177.6° in the tetragonal structure but χ_1 = −65.7° in the triclinic crystal structure.

Attempts to extend the coupling constant calculations and χ_1 angle comparison to additional crystal structures of a lower resolution [e.g., the monoclinic 2.5Å resolution structure (Rao et al., 1983)] showed that there are major differences between the χ_1 angles in these and the tetragonal and triclinic crystal structures for residues with both averaged and nonaveraged $^{3}J_{\alpha\beta}$ values. For example, in the comparison of the monoclinic and type 2 tetragonal crystal structures, 62% of the side chains

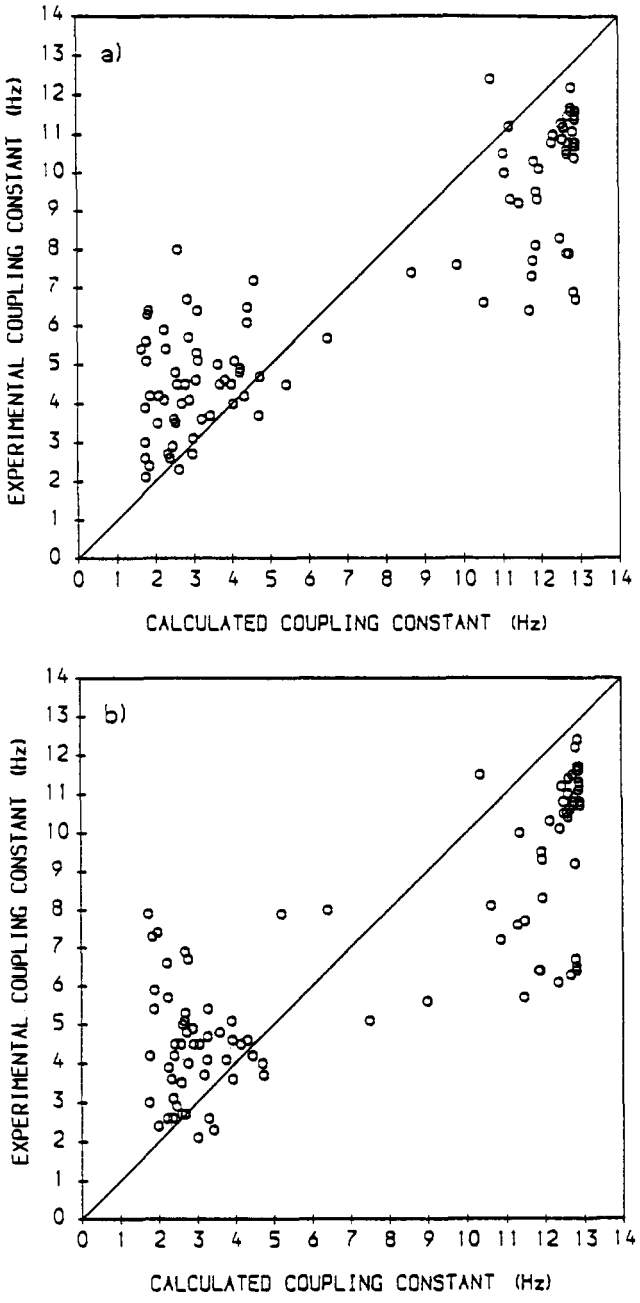

FIGURE 4: Plots of the experimental $C^{\alpha}H-C^{\beta}H$ coupling constants versus the calculated coupling constants for $^3J_{\alpha\beta}$ values calculated by using (a) χ_1 torsion angles from the tetragonal type 2 crystal structure and (b) χ_1 torsion angles from the triclinic crystal structure of hen lysozyme. For residues where the β-methylene protons have not been stereospecifically assigned, the calculated coupling constants are plotted against the experimental coupling constants so as to give the the best agreement.

with nonaveraged $^3J_{\alpha\beta}$ values occupy different rotamers in the two structures. The lower resolution of these structures is, therefore, not sufficient to define the side-chain conformations sufficiently accurately for the purpose of comparison with the NMR data.

An examination of the environments of the side chains of the residues for which $^3J_{\alpha\beta}$ values are available in the crystal structures shows that almost all the residues found to have large discrepancies between the calculated and experimental $C^{\alpha}H-C^{\beta}H$ coupling constants have exposed positions at the protein surface, with the side chains clearly extending out into the surrounding medium (see Figure 5). The only exception is Val 99, which has an interior position in the protein structure; this residue is discussed further below. Interestingly, the side chains of two of the residues with multiple conformations in solution, Glu 7 and Arg 68, are found in the tetragonal, but not the triclinic, crystal structure to be hydrogen bonded, to Gly 4 and Thr 51, respectively. If these hydrogen bonds are present in solution they do not constrain the side-chain conformations to a single minimum. It seems likely, therefore, that either they are not present in solution or that they are weak and are only present in one of the multiple side-chain conformations adopted in the solution structure. The residues where we do not see large-scale averaging of coupling constants have a range of positions in the structure. Many are quite buried, but a few, such as Asp 18 and Asn 65, are in positions that are as exposed as the majority of those in the earlier category. In these cases interactions with neighboring groups are presumably sufficient to stabilize one conformation significantly relative to the others. There is no apparent difference, however, in the correlation between the experimental and calculated $^3J_{HN\alpha}$ data for residues with or without rotationally disordered side chains.

In order to probe the environment of the side chains more systematically, solvent accessibility calculations were performed for the tetragonal and triclinic crystal structures by using the method of Richmond and Richards (1978). The percentage exposure of the side chains (the surface area of the side-chain atoms accessible to water in the lysozyme molecule compared to the accessible surface area of the same side chain in a fully extended conformation) were calculated for all the residues. The results for the tetragonal crystal structure are shown in Figure 6; the data for the triclinic structure are closely similar. The distribution of values confirms that the side chains where we see extensive motional averaging generally have a high percentage of solvent exposure (62% of the side chains in both crystal structures having values greater than 60%), while lower percentage exposure values dominate for side chains where we see no large-scale averaging of coupling constants (only 14% of these residues in the tetragonal and 17% in the triclinic structures having values above 60%).

This analysis indicates that in the interior of the protein the majority of side chains have a well-defined conformation about χ_1 in solution, which is accurately represented by the crystallographic χ_1 values. In contrast, 55% of the residues studied with a side-chain solvent accessibility greater than 60% adopt multiple conformations and hence are undergoing large-scale motions in solution. An exception to this generalization appears to be Val 99, which has an experimental $^3J_{\alpha\beta}$ value of 6.3 Hz but an interior position in the structure and a side-chain solvent accessibility of zero. Here, as there is only one proton attached to the β carbon, the experimental coupling constant value could represent the presence of an unusual conformation about χ_1 rather than motional averaging. A comparison of the χ_1 values in the two crystal structures shows, however, that the residue occupies different staggered conformations in the tetragonal and triclinic crystal forms (χ_1 = 171.1° in the triclinic and 80.3° in the tetragonal). It is probable therefore that the side chain of this residue adopts multiple conformations in solution; 50% population of these two conformers would give, using the Karplus equation, a predicted $^3J_{\alpha\beta}$ value of 7.3 Hz. Additional evidence in support of this interpretation of the coupling constant value comes from the observation that the two $NH-C^{\gamma}H_3$ NOE's are found to have closely similar intensities. Distances from the tetragonal crystal structure predict that the $NH-C^{\gamma 1}H_3$ NOE should be more intense than the $NH-C^{\gamma 2}H_3$ NOE (NH to CH_3 distance 2.9 Å for γ_1 and 4.4 Å for γ_2), while the triclinic crystal structure predicts the converse (i.e., $NH-C^{\gamma 2}H_3$ should be more intense than NH–

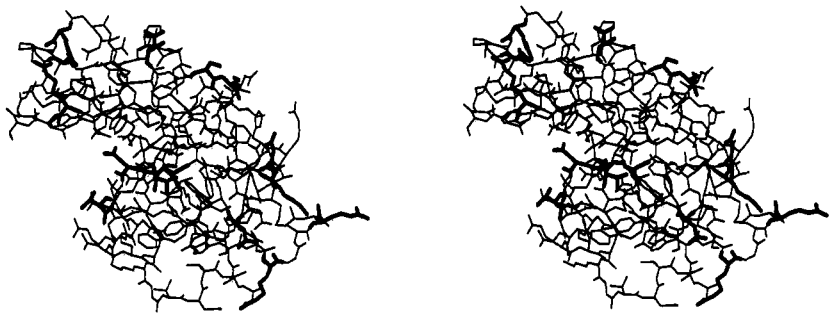

FIGURE 5: Stereodiagram of the tetragonal type 2 crystal structure of hen lysozyme with the residues with motionally averaged $^3J_{\alpha\beta}$ values shown by bold lines.

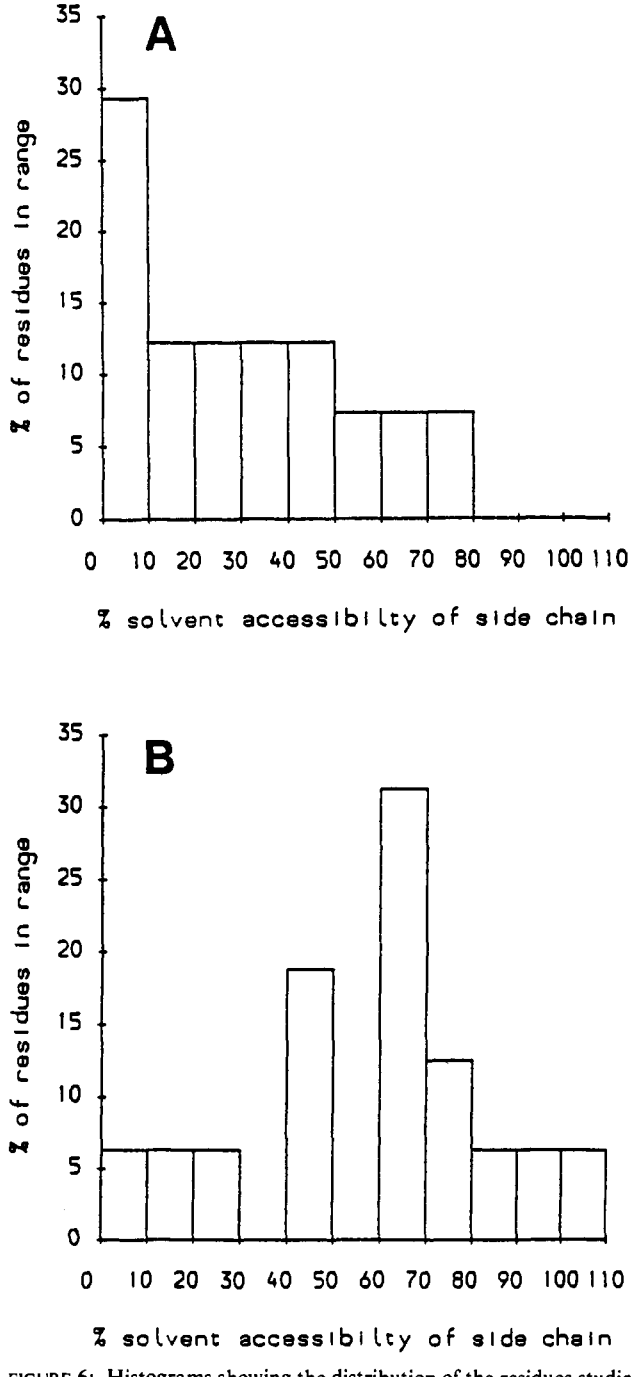

FIGURE 6: Histograms showing the distribution of the residues studied in categories of side-chain solvent accessibility in the tetragonal type 2 crystal structure for (A) the 41 residues where the $^3J_{\alpha\beta}$ values are consistent with a single staggered conformation about χ_1 and (B) the 16 residues with $^3J_{\alpha\beta}$ values averaged by the population of multiple conformations.

$C^{\gamma_1}H_3$; distances 4.6 Å for γ_1 and 2.7 Å for γ_2).

Unless multiple occupancies are specifically identified in a crystal structure, information about distributions of side-chain conformers comes from crystallographic temperature factors. Examination of the available temperature factors for tetragonal type 2 crystal structure shows that for residues identified as having a single conformational state about χ_1 in solution, the temperature factors of the γ atoms are in general low and comparable in size with the temperature factors for main-chain atoms. For the residues with motionally averaged $C^\alpha H$–$C^\beta H$ coupling constants a significant proportion of the residues have substantially higher γ-atom temperature factors; 50% of the residues, compared with only 7% for residues occupying a single conformation, have γ-atom temperature factor values greater than 30 Å^2 (see Figure 7). In these cases there is therefore evidence for rotational disorder about χ_1 in the crystal structure as well as in the solution structure. Rotational disorder for side chains in crystals of lysozyme has been previously identified specifically from crystallographic data for four residues (Arg 73, Val 109, Arg 125, and Arg 128) (Grace, 1980). Three of these residues have been investigated here, Val 109, Arg 125, and Arg 128; in all cases the $^3J_{\alpha\beta}$ values are found to be motionally averaged. It is, however, interesting to look at the cases with averaged $C^\alpha H$–$C^\beta H$ coupling constant values but low temperature factors for the γ position. In three of the five cases with temperature factors for the γ atom less than 20 Å^2 (Lys 13, Asn 37, and Arg 68) there are high temperature factors (greater than 30 Å^2) for atoms further out along the side chains, suggesting that even in these cases rotational disorder does occur in the crystal but that, in contrast to the solution case, it is restricted to the extremities of the side chains.

Discussion

This analysis of torsion angles derived from coupling constant measurements has demonstrated that there are significant differences between the interior and the surface of the protein. The data show that, in solution, in the interior of the protein both the main-chain and the side-chain atoms have well-defined conformations. The side chains are predominantly in staggered conformations and they appear to undergo only small fluctuations about their average χ_1 value. An exception in the case of lysozyme is Val 99, the side chain of which seems to adopt multiple conformations despite the interior position of the residue. Comparison with ϕ and χ_1 angles from high-resolution crystal structures shows that there is a good correlation, for both main-chain and side-chain atoms, between the conformation in solution and in crystals. The situation for residues located near the surface of the protein is, however, very different. The main chain ϕ torsion angles are still well defined and the $^3J_{HN\alpha}$ values are in agreement with crystallographic data, but many of the side chains adopt multiple

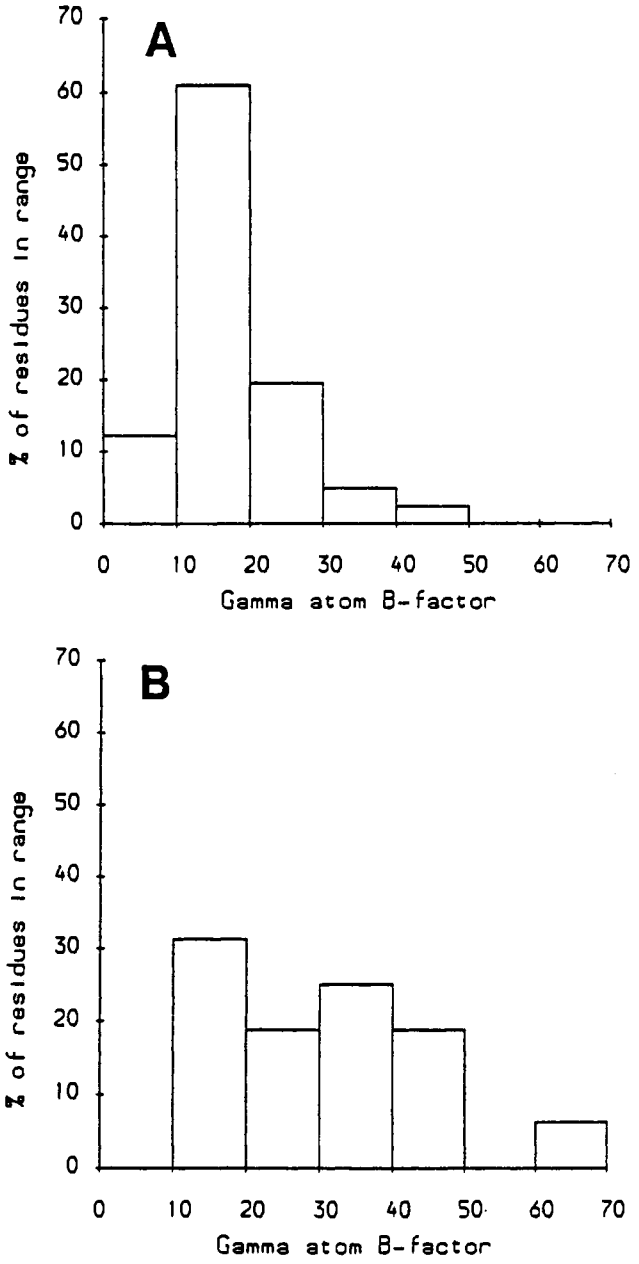

FIGURE 7: Histograms showing the percentage of the residues studied with a given temperature factor for the γ position in the tetragonal type 2 crystal structure for (A) the 41 residues where the $^3J_{\alpha\beta}$ values are consistent with a single staggered conformation about χ_1 and (B) the 16 residues with $^3J_{\alpha\beta}$ values averaged by the population of multiple conformations.

conformational states about χ_1 as indicated by extensive averaging of $^3J_{\alpha\beta}$ values. This conformational variability of surface groups in solution is underestimated by studying an individual crystal structure, but the data presented here suggest that it may perhaps be revealed by a survey of structures in different crystalline forms of the protein. The apparent difference in the dynamic properties in solution and crystals, or indeed in different crystal structures, is also indicated by differences in hydrogen-exchange behavior recently reported for lysozyme (Pedersen et al., 1990).

It is interesting to compare these results with those predicted from molecular dynamics simulations (Hoch et al., 1985; Dobson & Karplus, 1986). In these simulations the time-average coupling constants were compared with those computed from the average structure of the protein obtained from the simulations. These values correspond to the experimental coupling constants and those calculated from the torsion angles observed in the crystal structure, respectively. Excluding cases where the side chain occupies multiple conformations, the simulations predict that the gradient of the least-squares line fitted to the data will be 0.89 for coupling constants corresponding to ϕ and 0.88 for those corresponding to χ_1. Comparison of these values with the experimental data presented here (gradients of 0.99 for ϕ and 0.74 for χ_1) shows that for the main chain the actual fluctuations about the average ϕ torsion angle appear to be smaller than those predicted by the simulations. This observation could, however, be an artifact resulting from the *A*, *B*, and *C* parameters used in the Karplus equation. The parameters were obtained from a fit of experimental BPTI coupling constants to the X-ray ϕ angles (Pardi et al., 1984) and they will therefore already take into account the backbone dynamics of BPTI in solution. The gradient of 0.99 obtained for lysozyme could reflect that this protein has similar dynamical behavior in solution to BPTI.[2] For side chains about χ_1 there is a poorer experimental correlation, which could result from the parameters used in the Karplus equation or could reflect larger experimental fluctuations about χ_1 than predicted. It will be of particular interest, in the light of these data, to explore ways of extending the experimental analysis to other torsion angles (χ_2, χ_3, ...); the molecular dynamics simulations predict that motional averaging will increase significantly as the number of bonds from the main chain increases (Hoch et al., 1985).

The data presented in this paper are for a compact and highly stable globular protein. Many proteins are substantially less ordered than lysozyme (Williams, 1989; Dobson, 1989), and the dynamic properties of linker regions in multidomain and multisubunit proteins represent more extreme examples of the conformational variability of even main-chain regions that are not in a tightly folded structure (Perham et al., 1987; Oswald et al., 1989). In addition the cooperative unfolding of a protein, even to the relatively closely packed molten globule state detected in the protein α-lactalbumin, closely related to lysozyme, appears from chemical shift values to generate a high degree of disorder for side chains even in presence of ordered secondary structure (Baum et al., 1989). It is thus apparent that the close packing of side chains is required to constrict them into single conformational states. Even here, though, the barriers to rotation can be low as revealed, for example, by the motional properties of symmetric side chains in proteins such as the aromatic rings of phenylalanine and tyrosine residues (Campbell et al., 1985).

The rotational disorder in the side chains of many surface residues observed for lysozyme needs to be taken into account in detailed analysis of protein structures, in model building, in mechanistic studies, and in calculations (e.g., of electrostatic potentials) if realistic conclusions are to be made. It also has to be taken into account when considering the reliability of stereospecific assignments and the interpretation of NOE's in terms of the three-dimensional structure. Given the vital role of surface residues in the biological functions of proteins, NMR analyses of the type detailed here should have particular importance.

ACKNOWLEDGMENTS

We thank Professor Sir David Phillips for permission to use his crystal coordinate set for tetragonal crystals and Dr. Sax

[2] A combined set of 207 $^3J_{HN\alpha}$ values from hen lysozyme (this paper) and human lysozyme (Redfield & Dobson, 1990) together with 46 $^3J_{HN\alpha}$ values for BPTI (Pardi et al., 1984) have been used in a fitting procedure to obtain values of 6.0, −1.4, and 2.4 for the parameters *A*, *B*, and *C* in the Karplus equation.

Mason who provided us with the coordinates of the lysozyme structure in triclinic crystals. C.M.D. and C.R. are members of the Oxford Centre for Molecular Sciences which is supported by SERC and MRC.

Supplementary Material Available

A table of corrected NH–C$^{\alpha}$H coupling constants for hen lysozyme at 35, 45, and 55 °C (6 pages). Ordering information is given on any current masthead page.

Registry No. Lysozyme, 9001-63-2.

References

Anil, K., Ernst, R. R., & Wüthrich, K. (1980) *Biochem. Biophys. Res. Commun. 95*, 1.

Arseniev, A., Schultze, P., Wörgötter, E., Braun, W., Wagner, G., Vašák, M., Kägi, J. H. R., & Wüthrich, K. (1988) *J. Mol. Biol. 201*, 637.

Aue, W. P., Bartholdi, E., & Ernst, R. R. (1976) *J. Chem. Phys. 64*, 2229.

Baum, J., Dobson, C. M., Evans, P. A., & Hanley, C. (1989) *Biochemistry 18*, 7.

Bax, A., & Freeman, R. (1981) *J. Magn. Reson. 44*, 542.

Billeter, M., Kline, A. D., Braun, W., Huber, R., & Wüthrich, K. (1989) *J. Mol. Biol. 206*, 677.

Blake, C. C. F., Mair, G. A., North, A. C. T., Phillips, D. C., & Sarma, V. R. (1967) *Proc. R. Soc. London, B 167*, 365.

Blundell, T. L., & Johnson, L. N. (1976) *Protein Crystallography*, Academic Press, New York.

Campbell, I. D., Dobson, C. M., & Williams, R. J. P. (1975) *Proc. R. Soc. London A 345*, 41.

Campbell, I. D., Dobson, C. M., & Williams, R. J. P. (1985) *Biochem. J. 231*, 1.

Clore, G. M., & Gronenborn, A. M. (1987) *Protein Eng. 1*, 275.

Delepierre, M., Dobson, C. M., & Poulsen, F. M. (1982) *Biochemistry 21*, 4756.

de Marco, A., Llinás, M., & Wüthrich, K. (1978) *Biopolymers 17*, 617.

Dobson, C. M. (1989) in *Protein Structure and Engineering* (Jardetzky, O., Ed.) p 193, Plenum Press, New York.

Dobson, C. M., & Karplus, M. (1986) *Methods Enzymol. 131*, 362.

Grace, D. E. P. (1980) Ph.D. Thesis, Oxford University.

Griesinger, C., Sørensen, O. W., & Ernst, R. R. (1987) *J. Magn. Reson. 75*, 474.

Handoll, H. H. G. (1985) Ph.D. Thesis, Oxford University.

Hoch, J. C., Dobson, C. M., & Karplus, M. (1985) *Biochemistry 24*, 3831.

Hodsdon, J. M., Sieker, L. C., & Jensen, L. H. (1975) *Am. Crystallogr. Assn. Abstr. 3*, 16.

Hyberts, S. G., Märki, W., & Wagner, G. (1987) *Eur. J. Biochem. 164*, 625.

IUPAC-IUB Commission on Biochemical Nomenclature (1970) *J. Mol. Biol. 52*, 1.

Jeener, J., Meier, B. H., Bachmann, P., & Ernst, R. R. (1979) *J. Chem. Phys. 71*, 4546.

Karplus, M. (1959) *J. Chem. Phys. 30*, 11.

Kay, L. E., Torchia, D. A., & Bax, A. (1989) *Biochemistry 28*, 8972.

Kopple, K. D., Wiley, G. R., & Tauke, R. (1973) *Biopolymers 12*, 627.

Leatherbarrow, R. J., & Fersht, A. R. (1986) *Protein Eng. 1*, 7.

Macura, S., Huang, Y., Suter, D., & Ernst, R. R. (1981) *J. Magn. Reson. 43*, 259.

Mason, S. A., Bentley, G. A., & McIntyre, G. J. (1984) in *Neutrons in Biology* (Schoenborn, B. P., Ed.) p 323, Plenum Press, New York.

Nagayama, K., & Wüthrich, K. (1981) *Eur. J. Biochem. 115*, 653.

Neuhaus, D., Wagner, G., Vašák, M., Kägi, J. H. R., & Wüthrich, K. (1985) *Eur. J. Biochem. 151*, 257.

Oswald, R. E., Bogusky, M. J., Bamberger, M., Smith, R. A. G., & Dobson, C. M. (1989) *Nature 337*, 579.

Pardi, A., Billeter, M., & Wüthrich, K. (1984) *J. Mol. Biol. 180*, 741.

Pedersen, T. G., Sigurskjold, B. W., Andersen, K. V., Kjaer, M., Poulsen, F. M., Dobson, C. M., & Redfield, C. (1990) *J. Mol. Biol.* (in press).

Perham, R. N., Packman, L. C., & Radford, S. E. (1987) *Biochem. Soc. Symp. 54*, 67.

Rance, M., Sørensen, O. W., Bodenhausen, G., Wagner, G., Ernst, R. R., & Wüthrich, K. (1983) *Biochem. Biophys. Res. Commun. 117*, 479.

Rao, S. T., Hogle, J., & Sundaralingam, M. (1983) *Acta Crystallogr. C39*, 237.

Redfield, C., & Dobson, C. M. (1988) *Biochemistry 27*, 122.

Redfield, C., & Dobson, C. M. (1990) *Biochemistry 29*, 7201.

Richmond, T. J., & Richards, F. M. (1978) *J. Mol. Biol. 119*, 537.

Smith, J. L., Hendrickson, W. A., Honzatko, R. B., & Sheriff, S. (1986) *Biochemistry 25*, 5018.

States, D. J., Haberkorn, R. A., & Ruben, D. J. (1982) *J. Magn. Reson. 48*, 286.

Wagner, G., & Wüthrich, K. (1986) *Methods Enzymol. 131*, 307.

Wagner, G., Braun, W., Havel, T. F., Schaumann, T., Gō, N., & Wüthrich, K. (1987) *J. Mol. Biol. 196*, 611.

Williams, R. J. P. (1989) *Eur. J. Biochem. 183*, 479.

Wüthrich, K. (1986) *NMR of Proteins and Nucleic Acids*, Wiley, New York.